



Cite this: *Phys. Chem. Chem. Phys.*, 2019, 21, 16798

Revealing the switching mechanisms of an off–on–off fluorescent logic gate system†

Weijie Chi,^a Jie Chen,^b Qinglong Qiao,^b Ying Gao,^{ac} Zhaochao Xu^{ib} and Xiaogang Liu^{id}*^a

A deep understanding of fluorescence on–off and off–on switching mechanisms is the foundation for rationally designing highly effective molecular logic gate components and systems. These mechanisms, however, are often subtle to perceive and interpret, as multiple effects may contribute to the change of fluorescence signals. Herein, we systematically investigated the ‘off–on–off’ switching mechanisms of a fluorescent logic gate molecule **M1** using density functional theory (DFT) and time-dependent DFT (TD-DFT). Based on photoexcitation and photoemission calculations, and potential energy surface scans in the excited state, we have shown that as the pH of the medium continuously decreases and the sequential protonation of the molecule takes place, the prevention of twisted intramolecular charge transfer (TICT) followed by the activation of photo-induced electron transfer (PET) was responsible for the off–on–off switching mechanism of **M1**. Our results provided new insights for understanding the ‘off–on–off’ phenomenon in **M1**. The good agreement between theoretical calculations and experimental observations also suggests that computational chemistry is a powerful tool to aid the molecular design and engineering of fluorescent logic gate compounds.

Received 12th March 2019,
Accepted 13th July 2019

DOI: 10.1039/c9cp01401b

rsc.li/pccp

1 Introduction

Fluorescent molecular logic gates have attracted considerable research interest, because of their important applications in chemical computing, bioimaging, biosensing and therapeutic technologies.^{1–6} Since the seminal work of de Silva and co-workers,⁶ many logic gates, *i.e.*, AND, OR, INHIBIT, NOR, and XOR, have been developed based on various molecules.^{3,5,7,8} These molecular logic gates are usually based on fluorescent probes that change fluorescence intensities and/or colors in response to various chemical inputs.⁹

Among these chemical inputs, pH represents one key input to modulate fluorescence output in many molecular logic gates. For example, the first molecular logic operation reported by de Silva in 1993 employs pH to change the emission intensities of an anthracene fluorophore.⁶ In recently years, due to the advantages of facile synthesis, ease of derivations, and good optical properties, naphthalimide and its derivatives have been

widely employed in the construction of multi-stimuli molecular logic gates with significant responses to protons, metal ions, and organic molecules.^{10–14} Notably, Georgiev and coworkers designed and synthesized 1,8-naphthalimide bichromophore as a four-input Disabled-Enabled-OR logic gate.¹⁵ This system supports reversible operations in both Disable and Enable modes. Shen *et al.* developed a dyad, consisting of naphthalimide and spiroopyran units.¹⁶ This dyad employs protonation, deprotonation, UV irradiation and Fe³⁺ as inputs and emission intensity as an output. Recently, Magri *et al.* reported many fluorescent AND logic gate systems based on various inputs.^{17–21} To date, simple ‘turn-on’ and ‘turn-off’ fluorescence switches as a result of pH modulations have been reported abundantly in the literature.¹⁸

However, the design of more complex signal responses, such as ‘on–off–on’ or ‘off–on–off’ switches, remains a challenging task.^{19–23} A common design strategy to realize such complex responses is to combine two antagonistic proton receptors, typically by turning on/off the photo-induced electron transfer (PET) mechanism. Classical PET (Scheme 1a), including both acceptor-PET (a-PET) and donor-PET (d-PET) processes, can be described as an electron transfer, caused by the absorption of light, from an electron-rich fragment (the donor, D) to an electron deficient fragment (the acceptor, A) under the condition of proper matching of energy levels. Recently, Pischel and coworkers reported an ‘off–on–off’ T-latch fluorescence switching **M1** (Scheme 1b) based on a naphthalimide fluorophore.²⁴

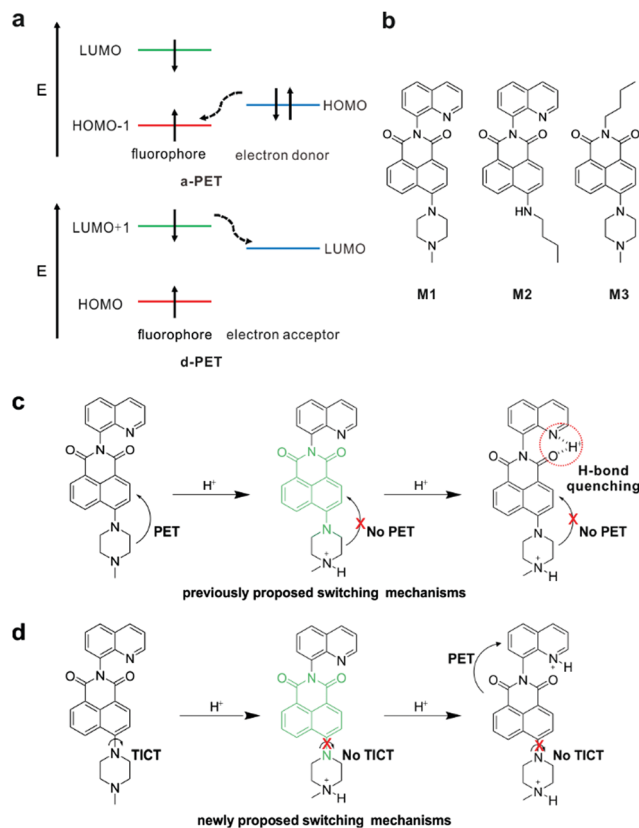
^a Science and Math Cluster, Singapore University of Technology and Design, 8 Somapah Road, Singapore 487372, Singapore.

E-mail: xiaogang_liu@sutd.edu.sg

^b CAS Key Laboratory of Separation Science for Analytical Chemistry Dalian Institute of Chemical Physics, Chinese Academy of Sciences, 457 Zhongshan Road, Dalian 116023, China

^c Jilin Engineering Normal University, Changchun, 130052, China

† Electronic supplementary information (ESI) available. See DOI: 10.1039/c9cp01401b



Scheme 1 (a) Transition molecular orbitals in the PET process, with transitions in the excited states, (b) molecular structures of **M1**, **M2**, and **M3**, (c) previously proposed switching mechanism of **M1** by Pischel and co-workers, and (d) newly proposed switching mechanism of **M1** in this work.

They ascribed the first-stage off-on response of this switching to the prevention of PET upon the addition of the first proton to the piperazine-naphthalimide moiety, and assigned the following on-off response to enhanced hydrogen bond effects after the addition of the second proton (Scheme 1c). In contrast, A. P. de Silva's group proposed that the formation of a non-emissive twisted internal charge transfer (TICT) excited state might be the fluorescence quenching mechanism of piperazine-naphthalimide derivatives.²⁵ Unfortunately, they did not provide direct experimental data to support their viewpoints. The molecular origin of pH-dependent responses in T-latch **M1** thus remains obscure.

With the rapid development of computational chemistry and computer technologies, exploring molecular properties in the excited states has become possible. These calculations could provide important insights in understanding the fluorescence turn-on/off mechanisms and shed light on the rational design of molecular logic gates with complex operations/responses.²⁰ In this work, we have investigated the photo-physical properties of **M1** along with reference compounds **M2** and **M3**, using density functional theory (DFT) and time-dependent DFT (TD-DFT), in order to reveal the 'off-on-off' switching mechanisms of **M1**. Our results showed that the TICT mechanism, as proposed by A. P. de Silva, is responsible for the

off-on switching of **M1** upon the addition of the first proton (Scheme 1d). We also found that PET results in the on-off switching of the protonated **M1** upon the addition of the second proton (Scheme 1d). This newly proposed mechanism leads to a deep understanding of the working principle of **M1**, and demonstrates that multiple fluorescence mechanisms can be collectively employed to construct molecular logic gates with complex operations.

2 Experimental and computation methods

Geometry optimizations were carried out at the M062X/Def2svp level.^{26,27} Solvation effects were taken into account using the SMD model.²⁸ We used acetonitrile (to be consistent with the experimental conditions of Pischel and coworkers) as well as water as solvents. Frequency calculations were performed to confirm that we obtained stable structures without imaginary vibration frequencies. The excitation energies and emission energies of all molecules were calculated using state-specific equilibrium solvation, unless stated otherwise.²⁹ The potential energy surface (PES) in the first excited state (S_1) was calculated at the same level using relaxed scans around the bond connecting the amino group to the naphthalimide moiety. All DFT and TD-DFT calculations were carried out using Gaussian 16A.³⁰ The molecular excitation properties were also investigated by the hole-electron analysis using Multiwfn 3.6.³¹ Previous studies showed that the M062X functional was suitable for calculating the excited-state PES where significant variations in charge transfer were involved, although it consistently over-estimated photo-excitation/deexcitation energy.³² M062X has also been frequently used to explain the luminescence mechanisms of organic dyes with satisfying results.^{33–35}

To experimentally validate the newly proposed quenching mechanism in logic gate molecules, we synthesized and characterized molecule **M3**. 75 mg (0.75 mmol, 5 eq.) of *N*-methyl piperazine was added dropwise to a solution of 50 mg (0.15 mmol) of *N*-butyl-4-bromo-1,8-naphthalimide in 5 mL of 2-methoxyethanol. The mixture was heated at 120 °C for 5 h, while being monitored *via* thin layer chromatography. After the reaction was completed, the solution was removed under reduced pressure and the crude product was then purified *via* column chromatography to give **M3** as a yellow solid in 66% yield (35 mg). ¹H-NMR (400 MHz, CDCl₃) δ 8.58 (dd, $J = 7.3, 0.9$ Hz, 1H), 8.51 (d, $J = 8.0$ Hz, 1H), 8.40 (dd, $J = 8.4, 0.9$ Hz, 1H), 7.72–7.64 (m, 1H), 7.22 (d, $J = 8.1$ Hz, 1H), 4.20–4.14 (m, 2H), 3.38–3.25 (m, 4H), 2.75 (s, 4H), 2.44 (s, 3H), 1.71 (ddd, $J = 12.5, 8.5, 6.6$ Hz, 2H), 1.44 (dq, $J = 14.7, 7.4$ Hz, 2H), 1.01–0.93 (m, 3H) (Fig. S1, ESI[†]).

3 Results and discussion

3.1 Off-on mechanism of **M1**

The fluorescence quantum yields of **M1–M3** are 0.017, 0.560, and 0.018 in acetonitrile solution, respectively. Pischel *et al.*

inferred that the low quantum yields of **M1** and **M3** before protonation were due to the presence of PET. During the PET process, an electron transferred from the methyl-substituted piperazinyl group to the naphthalimide unit upon photoexcitation, thus quenching the fluorescence of **M1** and **M3**. Subsequent additions of one proton to **M1/M3** could block PET and turn on the fluorescence. For **M2**, Pischel speculated that protonation leads to the transformation of the quinolinyl residue into a quinolinium cation, and the fluorescence is quenched by strong hydrogen-bonding interactions between NH^+ and the imide carbonyl $\text{C}=\text{O}$ moiety. The hydrogen bond quenching (HBQ) mechanism can also be found in **M1** upon the addition of the second proton. While Pischel developed one excellent molecular logic gate, they did not provide compelling experimental proof to support the proposed mechanisms.

We decided to explore the working mechanism of **M1–M3** with the help of theoretical chemistry. Because **M1** contains two receptors (a piperazinyl and a quinolinyl group), it can be considered as a ‘structural combination’ of **M2** and **M3**. In other words, the two-step off-on-off responses of **M1** represent the sensing mechanism of **M2** and **M3**, respectively.

We first determined the relative energy preference of various protonation sites in **M1**. Fig. 1a shows five possible positions and the relative Gibbs free energies of the corresponding protonated products. Clearly, the N atom at Site I has the highest reactivity towards protonation, due to the lowest Gibbs free energy. The next energetically favorable protonation site resides at Site II (Fig. S2, ESI[†]). Therefore, **M1-1H** (Fig. 1b) is regarded as the product formed upon the addition of the first proton and **M1-2H** (Fig. 1b) is that for the addition of the second proton in this work.

We continued to explore the ‘off-on’ mechanism from **M1** to **M1-1H**. TD-DFT calculations based on the ground-state structure (Fig. 1c) show that 97% of the orbital transition contribution comes from the highest occupied molecular orbital (HOMO) to the lowest unoccupied molecular orbital (LUMO) in **M1** upon photoexcitation to the S_1 state. Moreover, both the HOMO and the LUMO are located in the naphthalimide moiety. Subsequent hole–electron analysis also shows that both the hole and the electron of **M1** are distributed in the naphthalimide unit. The moderate overlap between hole and electron and the short distance of the electron/hole centroid^{31,36} demonstrate a weak intramolecular charge transfer feature in **M1** (Fig. S3, ESI[†]). We also noted that HOMO–1 is distributed in the methyl-substituted piperazinyl group. The energy difference between the HOMO and HOMO–1 is 0.53 eV. As there exist no quenching orbitals in the naphthalimide fluorophore, our results suggest that PET seems absent in **M1**. Indeed, TD-DFT calculations based on excited-state optimized structures suggest that the locally excited state $(\text{LE}_1)_{\text{min}}$ is a stable structure, before the methyl-substituted piperazinyl group rotates towards the TICT state (Fig. 1d). This $(\text{LE}_1)_{\text{min}}$ state is highly emissive with a large oscillator strength of 0.343.

After the protonation of **M1** to **M1-1H**, the main orbital transition during S_1 excitation is still from HOMO to LUMO (Fig. 1e), which is similar to that in **M1**. We also noted that

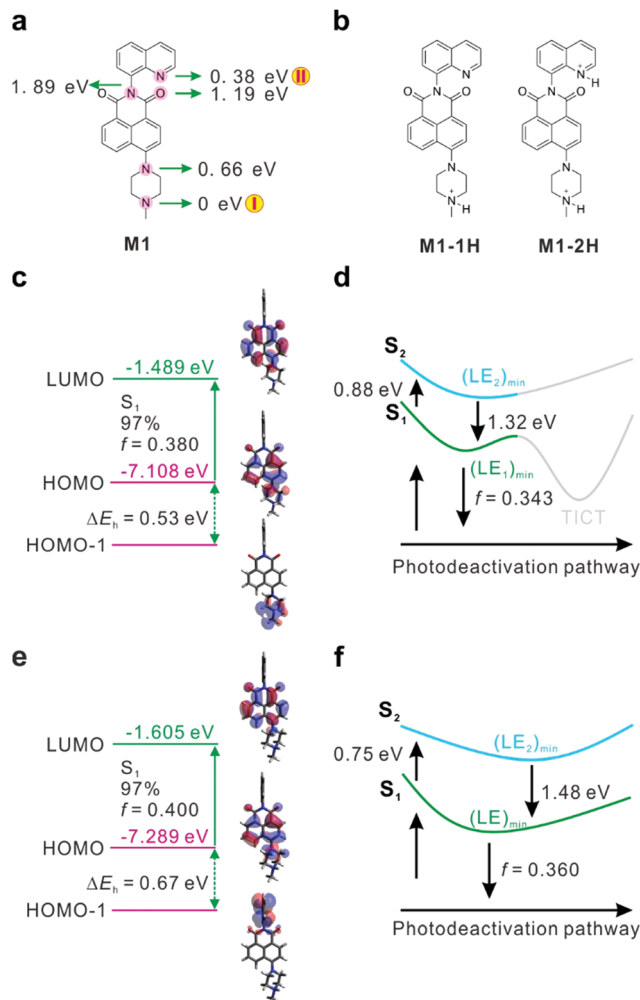


Fig. 1 (a) Five possible protonated positions and relative Gibbs free energy of protonated products, (b) molecular structures of protonated products, (c) molecular frontier orbitals and electronic transitions of **M1**, (d) illustration of the relative electronic energy between S_1 and S_2 of **M1**, (e) molecular frontier orbitals and electronic transitions of **M1-1H**, and (f) illustration of the relative electronic energy between S_1 and S_2 of **M1-1H**. For clarity, all energy levels are not drawn in scale. The vertical excitation energy was calculated using a linear solvation model, while de-excitation energy was computed using state-specific equilibrium solvation, all in acetonitrile.

HOMO–1 is distributed in the quinolinyl moiety in **M1-1H**, and the energy gap between HOMO and HOMO–1 increases to 0.67 eV. Compared with **M1**, molecule **M1-1H** exhibits a shorter distance between hole and electron centroids, and a larger overlap between hole and electron (Fig. S3, ESI[†]). This difference indicates that there is a smaller degree of intramolecular charge transfer in **M1-1H** than in **M1**. Moreover, highly emissive $(\text{LE}_1)_{\text{min}}$ remains the most stable S_1 structure in **M1-1H** (Fig. 1f). Similar electronic transition behaviors are also noted in **M3** in both the neutral and protonated states (Fig. S4, ESI[†]). According to these findings, the frontier orbitals in the methyl-substituted piperazinyl group are not involved in the photoexcitation of both **M1** and **M1-1H**. The calculated results are inconsistent with the previously proposed PET mechanism.

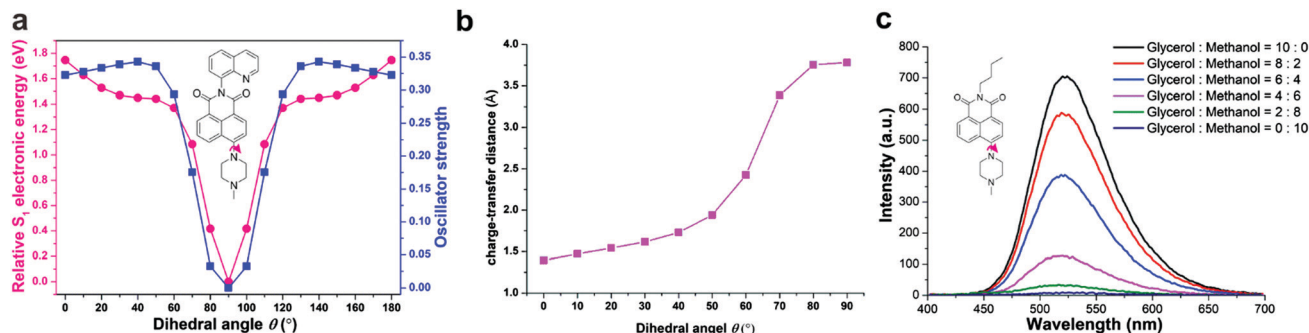


Fig. 2 (a) S_1 potential energy surface (pink) of **M1** and the corresponding oscillator strength (blue), as a function of the rotation of the methyl-substituted piperazinyl group in acetonitrile; the relative S_1 PES was calculated by setting $(S_1)_{\min}$ as the reference (0); (b) distance of charge transfer as a function of the rotation of the methyl-substituted piperazinyl group; (c) fluorescence spectra of **M3** in the glycerol/methanol mixture with different volume fractions of glycerol ($[M3] = 10 \mu\text{M}$).

To investigate the true molecular origins of weak emissions in **M1**, we calculated the geometric and electronic properties of the first excited states $(S_1)_{\min}$ after relaxation. In consideration of the strong electron-donating strength of the methyl-substituted piperazinyl group attached to the naphthalimide scaffold, we speculated that the strong push-pull effect may induce a structural twisting between the donor and acceptor moieties in the excited state, resulting in the formation of the TICT state in **M1**. We have thus constructed the PES of **M1** along the rotation of the piperazinyl group in the excited state (Fig. 2a). Moreover, we calculated the distance of charge transfer for every geometry along the twisting coordinate. Our results showed that the rotation of the piperazinyl group indeed leads to a $(S_1)_{\min}$ geometry and the distance of charge transfer consistently increases as the dihedral angle rises from 0 to 90° on the S_1 PES (Fig. 2b). At the most stable geometry, the methyl-substituted piperazinyl group is almost perpendicular to the naphthalimide unit. At this conformation, the LUMO is located on the naphthalimide unit, while the HOMO moves to the methyl-substituted piperazinyl group. This complete hole-electron separation leads to negligible oscillator strength ($f = 0$), indicating that this state is non-emissive.³⁷ Similarly, **M3** also exhibits a stable TICT configuration (Fig. S5, ESI[†]). These features are fully consistent with the TICT mechanism.

To further confirm TICT formation,^{38,39} the S_1 PES of **M1** was calculated using two range-separated hybrid functionals, CAM-B3LYP and ω B97XD, in acetonitrile (Fig. S6, ESI[†]). These results are in good agreement with the data derived from the M062X functional. Similar S_1 PESs favoring the formation of the TICT states were also obtained for **M1** and **M3** in water (Fig. S7, ESI[†]). In contrast, upon the protonation of the methyl-substituted piperazinyl group, our results show that TICT becomes energetically unfavorable in **M1-1H** (Fig. S8, ESI[†]).

We experimentally verified the TICT quenching mechanism by synthesizing and characterizing reference compound **M3**. Compound **M3** shows strong UV-vis absorption bands that maximize at 397 nm and 390 nm in methanol and glycerol, respectively (Fig. S9, ESI[†]). The corresponding fluorescence spectral peaks are located at 546 and 528 nm, respectively. Given that methanol and glycerol have similar solvent polarities, it is not surprising to observe these close UV-vis absorption

and fluorescence peaks. Notably, **M3** exhibited weak fluorescence (quantum yield = 0.007) in methanol. In stark contrast, strong emissions were observed in glycerol (quantum yield = 0.62). Accordingly, as we increased solvent viscosity by introducing more glycerol in the methanol/glycerol (Gly) mixtures (Fig. 2c), we noticed significant enhancements of fluorescence intensities by up to ~ 90 times in **M3**. This enhancement is ascribed to the blocked TICT rotations of the methyl-piperazine moiety in high viscosity solvents. These observations are fully consistent with our theoretical calculations.

We also performed the titration of **M3** with CF_3COOH to form protonated **M3-H** in methanol (Fig. S10, ESI[†]). Our results showed that **M3-H** exhibited bright emission and a blue shift of ~ 21 nm in the UV-vis absorption spectra as compared to that of **M3** (Fig. S10, ESI[†]). This pH-dependent large blue-shift in the UV-vis absorption spectra corresponds to the ICT mechanism, while no significant shift should be observed in the PET mechanism (as the quencher is isolated from the fluorophore).²³ This experimental evidence thus further disproves the PET mechanism and supports the TICT model.

In sum, both our computational and experimental results show that the fluorescence quenching of **M1** and **M3** derives from the formation of the TICT state instead of the PET mechanism.

3.2 On-off mechanism from **M1-1H** to **M1-2H**

Next, we studied the ‘on-off’ mechanism of **M1-H** upon the addition of the second proton (from **M1-1H** to **M1-2H**). We optimized the geometries of **M1-2H** both in the ground and excited state (Fig. 3a). In the ground state, the distances between the proton and two carbonyl oxygen atoms are 2.99 and 3.65 Å, respectively. These distances increase to 3.07 and 3.90 Å in the excited state. Clearly, these distances are longer than the van der Waals radius of hydrogen and oxygen atoms (2.6 Å), indicating the absence of hydrogen bond interactions.

These results contradict the mechanism of hydrogen bond interactions ($\text{N-H}^+ \cdots \text{O}$) as speculated by Pischel and co-workers in rationalizing the on-off switching from **M1-1H** to **M1-2H**. Our results also alert that one must take caution when interpreting specific intramolecular interactions based on the ‘two-dimensional’ canonical structures of a compound.

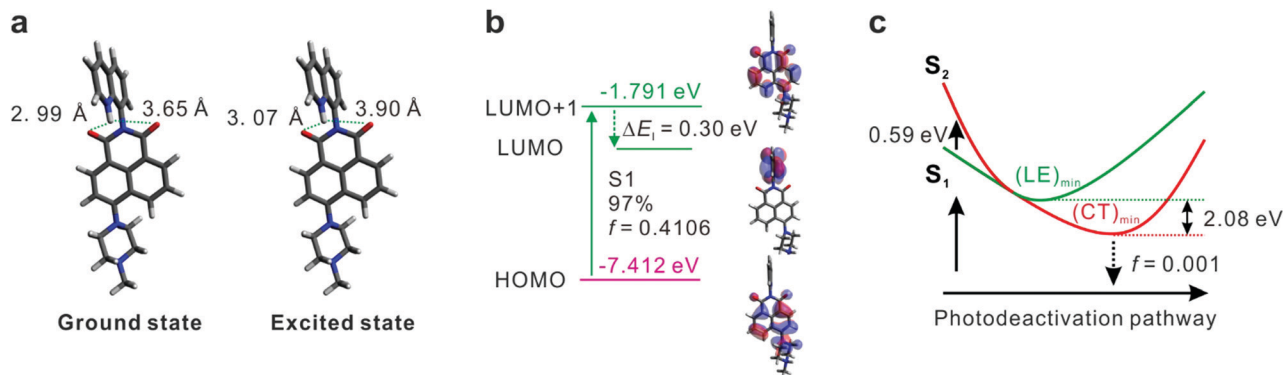


Fig. 3 (a) Geometric configurations and the distances of hydrogen and oxygen atoms for molecule **M1-2H** in both the ground and the excited states, (b) molecular frontier orbitals and electronic transitions of **M1-2H**, and (c) illustration of the relative electronic energy of S_1 and S_2 of **M1-2H** in acetonitrile. The vertical excitation energy was calculated using the linear solvation model, while de-excitation energy was computed using state-specific equilibrium solvation, all in acetonitrile. For clarity, all energy levels are not drawn to scale.

Based on the ground-state structure of **M1-2H**, we continued to calculate the excitation properties of **M1-2H** and rationalize the resulting fluorescence quenching. Our analysis showed that photoexcitation to the S_1 state is dominated by the transition from HOMO to LUMO+1 (Fig. 3c). We also observed a quenching orbital, LUMO, distributed in the quinolinyl moiety, and the gap between the LUMO and LUMO+1 is 0.30 eV. Clearly, the energy levels of these frontier molecular orbitals meet the requirement of d-PET. In addition, we have analyzed the TD-DFT results (S_1 and S_2) to study the fluorescence turn-off mechanism in **M1-2H**. Our results show that a state crossing between the LE and CT states exists in **M1-2H**, and the most stable S_1 structure corresponds to a CT state. This (CT)_{min} has a negligible oscillator strength ($f = 0.001$), thus explaining the complete quenching of fluorescence in **M1-2H**.

In sum, our results suggest that the ‘on-off’ switching from **M1-1H** to **M1-2H** should be attributed to the activation of the d-PET effect. After photoexcitation of **M1-2H**, the excited electron in LUMO+1 could quickly transfer to the LUMO (from the naphthalimide fragment to the protonated quinolinyl fragment), thus quenching the fluorescence and leading to a low quantum yield (0.017 in acetonitrile). The same quenching mechanism (d-PET) is also found in protonated **M2** (Fig. S11, ESI[†]).

4 Conclusions

We have performed detailed theoretical calculations to understand the pH-dependent fluorescence ‘off-on-off’ switching mechanism of a fluorescent molecular logic gate molecule **M1** (as well as reference compounds **M2** and **M3**). Our results did not support a previously proposed mechanism (PET followed by hydrogen bond interactions as pH continuously decreases). Instead, our computational and experimental studies showed that **M1** is prone to TICT formation, resulting in weak emission. Upon protonation of **M1** to form **M1-1H**, TICT is effectively suppressed, thus turning on bright fluorescence. However, further protonation activates d-PET in the resulting **M1-2H**, leading to another off state. Our results offer new insights into

the working mechanism of **M1** and suggest that multiple fluorescence on/off mechanisms can be combined to enable complex molecular logic gate operations in a single compound. The close agreement between experimental data and theoretical calculations also endorses the possibility of employing theoretical calculations to guide the rational design of fluorescent molecular logic gates in future work.

Conflicts of interest

There are no conflicts to declare.

Acknowledgements

WC and XL are grateful for the financial support from the Singapore University of Technology and Design (SUTD) and the SUTD-MIT International Design Centre (Grant No. T1SRCI17126, IDD21700101, and IDG31800104). ZX, JC, and QQ acknowledge the financial support from the National Natural Science Foundation of China (21878286 and 81772812) and DICP (No. DMTO201603 and TMSR201601). The authors would like to acknowledge the use of the High-Performance Computing (HPC) service of both the SUTD-MIT International Design Centre and the National Supercomputing Centre (Singapore) in carrying out this work.

Notes and references

- 1 K. Kompa and R. Levine, *Proc. Natl. Acad. Sci. U. S. A.*, 2001, **98**, 410–414.
- 2 D. C. Magri, G. J. Brown, G. D. McClean and A. P. de Silva, *J. Am. Chem. Soc.*, 2006, **128**, 4950–4951.
- 3 S. Erbas-Cakmak, S. Kolemen, A. C. Sedgwick, T. Gunnlaugsson, T. D. James, J. Yoon and E. U. Akkaya, *Chem. Soc. Rev.*, 2018, **47**, 2228–2248.
- 4 J. Axthelm, P. Hoffmann, N. Taye, S. Gläser, H. Görls, S. Hopkins, W. Plass, U. Neugebauer, S. Bonnet and A. Schiller, *J. Am. Chem. Soc.*, 2017, **139**, 4991–4994.

- 5 K. S. Park, C. Jung and H. G. Park, *Angew. Chem., Int. Ed.*, 2010, **122**, 9951–9954.
- 6 A. P. de Silva, H. Q. N. Gunaratne and C. P. McCoy, *Nature*, 1993, **364**, 42–44.
- 7 M. Massey, I. L. Medintz, M. G. Ancona and W. R. Algar, *ACS Sens.*, 2017, **2**, 1205–1214.
- 8 A. Lake, S. Shang and D. M. Kolpashchikov, *Angew. Chem., Int. Ed.*, 2010, **49**, 4459–4462.
- 9 S. Kou, H. N. Lee, D. van Noort, K. E. M. E. K. Swamy, S. H. Kim, J. H. Soh, K. M. Lee, S. W. Nam, J. Yoon and S. Park, *Angew. Chem., Int. Ed.*, 2008, **47**, 872–876.
- 10 M. de Sousa, M. Kluciar, S. Abad, M. A. Miranda, B. de Castro and U. Pischel, *Photochem. Photobiol. Sci.*, 2004, **3**, 639–642.
- 11 H. Wang, H. Wu, L. Xue, Y. Shi and X. Li, *Org. Biomol. Chem.*, 2011, **9**, 5436–5444.
- 12 J. Ling, G. Naren, J. Kelly, T. S. Moody and A. P. de Silva, *J. Am. Chem. Soc.*, 2015, **137**, 3763–3766.
- 13 M. Li, Z. Guo, W. Zhu, F. Marken and T. D. James, *Chem. Commun.*, 2015, **51**, 1293–1296.
- 14 D. C. Magri and J. C. Spiteri, *Org. Biomol. Chem.*, 2017, **15**, 6706–6709.
- 15 N. I. Georgiev, A. R. Sakr and V. B. Bojinov, *Sens. Actuators, B*, 2015, **221**, 625–634.
- 16 C. Zhao, Z. Wang, X. Gong, Q. Zhang, C. Wang and Y. Shen, *Dyes Pigm.*, 2017, **140**, 460–468.
- 17 J. C. Spiteri, A. D. Johnson, S. A. Denisov, G. Jonusauskas, N. D. McClenaghan and D. C. Magri, *Dyes Pigm.*, 2018, **157**, 278–283.
- 18 H. Yan, X. Meng, B. Li, S. Ge and Y. Lu, *J. Mater. Chem. C*, 2017, **5**, 10589–10599.
- 19 R. Zammit, M. Pappova, E. Zammit, J. Gabarretta and D. C. Magri, *Can. J. Chem.*, 2015, **93**, 199–206.
- 20 J. C. Spiteri, S. A. Denisov, G. Jonusauskas, S. Klejna, K. Szaciłowski, N. D. McClenaghan and D. C. Magri, *Org. Biomol. Chem.*, 2018, **16**, 6195–6201.
- 21 A. D. Johnson, K. A. Paterson, J. C. Spiteri, S. A. Denisov, G. Jonusauskas, A. Tron, N. D. McClenaghan and D. C. Magri, *New J. Chem.*, 2016, **40**, 9917–9922.
- 22 A. P. de Silva and H. Q. N. Gunaratne, *Chem. Commun.*, 1996, 2399–2400.
- 23 J. F. Callan, A. P. de Silva and N. D. McClenaghan, *Chem. Commun.*, 2004, 2048–2049.
- 24 V. F. Pais, P. Remón, D. Collado, J. Andréasson, E. Pérez-Inestrosa and U. Pischel, *Org. Lett.*, 2011, **13**, 5572–5575.
- 25 S. Zheng, P. M. Lynch, T. E. Rice, T. S. Moody, H. N. Gunaratne and A. P. de Silva, *Photochem. Photobiol. Sci.*, 2012, **11**, 1675–1681.
- 26 F. Weigend and R. Ahlrichs, *Phys. Chem. Chem. Phys.*, 2005, **7**, 3297–3305.
- 27 Y. Zhao and D. G. Truhlar, *Theor. Chem. Acc.*, 2008, **120**, 215–241.
- 28 A. V. Marenich, C. J. Cramer and D. G. Truhlar, *J. Phys. Chem. B*, 2009, **113**, 6378–6396.
- 29 R. Improta, V. Barone, G. Scalmani and M. J. Frisch, *J. Chem. Phys.*, 2006, **125**, 054103.
- 30 M. Frisch, G. Trucks, H. Schlegel, G. Scuseria, M. Robb, J. Cheeseman, G. Scalmani, V. Barone, G. Petersson and H. Nakatsuji, *et al.*, *Gaussian 16, Revision A. 03*, Gaussian Inc., Wallingford, CT, 2016.
- 31 T. Lu and F. Chen, *J. Comput. Chem.*, 2012, **33**, 580–592.
- 32 W. Chi, Q. Qiao, R. Lee, W. Liu, Y. S. Teo, D. Gu, M. J. Lang, Y.-T. Chang, Z. Xu and X. Liu, *Angew. Chem., Int. Ed.*, 2019, **58**, 7073–7077.
- 33 Q. Qi, W. Chi, Y. Li, Q. Qiao, J. Chen, L. Miao, Y. Zhang, J. Li, W. Ji and T. Xu, *Chem. Sci.*, 2019, **10**, 4914–4922.
- 34 Q. Qi, L. Huang, R. Yang, J. Li, Q. Qiao, B. Xu, W. Tian, X. Liu and Z. Xu, *Chem. Commun.*, 2019, **55**, 1446–1449.
- 35 L. Martinez-Fernandez, S. Arslançan, D. Ivashchenko, C. E. Crespo-Hernandez and I. Corral, *Phys. Chem. Chem. Phys.*, 2019, **21**, 13467–13473.
- 36 T. Le Bahers, C. Adamo and I. Ciofini, *J. Chem. Theory Comput.*, 2011, **7**, 2498–2506.
- 37 D. Escudero, *Acc. Chem. Res.*, 2016, **49**, 1816–1824.
- 38 A. Köhn and C. Hättig, *J. Am. Chem. Soc.*, 2004, **126**, 7399–7410.
- 39 P. Wiggins, J. G. Williams and D. J. Tozer, *J. Phys. Chem.*, 2009, **131**, 091101.